

COSMIC VOIDS

Nico Hamaus

Universitäts-Sternwarte München, Fakultät für Physik

Ludwig-Maximilians Universität München

Scheinerstr. 1, D-81679 München, Germany

Email: hamaus@usm.lmu.de

Web: www.usm.lmu.de/people/hamaus

Lecture notes for the *Lecture Series on Cosmology*,
held on June 29th 2017 at MPA in Garching.

Contents

1	Spherical evolution	3
1.1	Linear theory	3
1.2	Nonlinear theory	4
1.2.1	Overdensity	7
1.2.2	Underdensity	10
2	Excursion set theory	15
2.1	Overdensity	18
2.2	Underdensity	20
3	Clustering statistics	25
3.1	Void profile	25
3.2	Void model	28
4	Cosmology with voids	32
4.1	Redshift-space distortions	32
4.2	Alcock-Paczyński test	38
4.3	Weak lensing	38
4.4	Integrated Sachs-Wolfe effect	38

1 Spherical evolution

1.1 Linear theory

We will consider a density field $\rho(\mathbf{x}, t)$ at comoving coordinate \mathbf{x} and time t with a mean of $\bar{\rho}(t)$. The density contrast is defined as

$$\delta(\mathbf{x}, t) = \frac{\rho(\mathbf{x}, t)}{\bar{\rho}(t)} - 1 . \quad (1)$$

To linear order in the density contrast, conservation of mass implies

$$\frac{\partial \delta(\mathbf{x}, t)}{\partial t} + \frac{1}{a(t)} \nabla \cdot \mathbf{v}(\mathbf{x}, t) = 0 , \quad (2)$$

where a is the scale factor and \mathbf{v} the peculiar velocity field. The linear density contrast can be factorized into its temporal and spatial dependence via the linear growth factor $D(t)$,

$$\delta(\mathbf{x}, t) = D(t)\delta(\mathbf{x}) . \quad (3)$$

We can now write

$$\begin{aligned} \frac{\partial \delta(\mathbf{x}, t)}{\partial t} &= \frac{dD(t)}{dt} \delta(\mathbf{x}) = \frac{d \ln D(t)}{dt} \delta(\mathbf{x}, t) = \\ &= \frac{d \ln D(t)}{d \ln a(t)} \frac{d \ln a(t)}{dt} \delta(\mathbf{x}, t) = f(t) H(t) \delta(\mathbf{x}, t) , \end{aligned} \quad (4)$$

with the Hubble rate $H(t) \equiv \dot{a}(t)/a(t)$ and the linear growth rate $f(t) \equiv d \ln D(t)/d \ln a(t)$. Equation (2) can now be written as

$$\nabla \cdot \mathbf{v}(\mathbf{x}, t) = -f(t)a(t)H(t)\delta(\mathbf{x}, t) . \quad (5)$$

This can be integrated over some volume V ,

$$\int_V \nabla \cdot \mathbf{v}(\mathbf{x}, t) d^3x = -f(t)a(t)H(t) \int_V \delta(\mathbf{x}, t) d^3x . \quad (6)$$

On the left-hand side we apply the divergence theorem to convert the volume integral to a surface integral. Choosing a spherical surface $S = 4\pi r^2$ of a sphere of radius r and volume $V_S = \frac{4\pi}{3}r^3$, yields

$$\oint_S \mathbf{v}(\mathbf{x}, t) \cdot d\mathbf{S} = -f(t)a(t)H(t)\frac{4\pi}{3}r^3\Delta(r, t). \quad (7)$$

Here we defined the average density contrast within radius r as

$$\Delta(r, t) \equiv \frac{3}{4\pi r^3} \int_{V_S} \delta(\mathbf{x}, t) d^3x. \quad (8)$$

Finally, we obtain a relation between the radial velocity field and the average density contrast within the sphere [Peebles (1980)],

$$v(r, t) = -\frac{1}{3}f(t)a(t)H(t)r\Delta(r, t). \quad (9)$$

1.2 Nonlinear theory

In this section we will only consider spherically symmetric density fluctuations $\delta(r)$ with average density contrast

$$\Delta(r) = \frac{3}{r^3} \int_0^r \delta(r')r'^2 dr'. \quad (10)$$

For simplicity, we will also drop the explicit time dependence of most variables, unless necessary. The total mass inside a radius r is given by

$$M(r) = \frac{4\pi}{3}r^3\bar{\rho}[1 + \Delta(r)]. \quad (11)$$

Birkhoff's theorem (or Newton's shell theorem): "A spherically symmetric body affects external objects gravitationally as though all of its mass were concentrated at a point in its center". This means at any given distance r we only have to consider the mass $M(r) = M(< r)$ and can neglect the mass distribution at larger distances $M(> r)$. According to the Newtonian law of gravity, a test particle obeys the following equation of motion (here in

physical coordinates, not comoving),

$$\ddot{r} = -\frac{GM(r)}{r^2} . \quad (12)$$

Once integrated over time this gives

$$\frac{1}{2}\dot{r}^2 - \frac{GM(r)}{r} = K , \quad (13)$$

where the first term corresponds to the kinetic energy, the second term to the potential energy, and K is an integration constant. Plugging in equation (11) yields

$$\dot{r}^2 - \frac{8\pi G}{3}\bar{\rho}r^2 [1 + \Delta(r)] = 2K . \quad (14)$$

If we now define a critical density for the special case of $K = \Delta = 0$ (flat background),

$$\rho_c = \frac{3H^2}{8\pi G} , \quad (15)$$

where $\dot{r}/r = H = \dot{a}/a$ corresponds to the Hubble rate in this case. Further, we define $\Omega_m \equiv \bar{\rho}/\rho_c$ and write

$$\dot{r}^2 - \Omega_m H^2 r^2 [1 + \Delta(r)] = 2K . \quad (16)$$

The constant K can be determined by setting the initial conditions. Initially, density perturbations are very small, so we can use equation (9) to determine the initial total velocity, which is composed of Hubble flow and peculiar motion,

$$\dot{r}_i \simeq r_i H_i - \frac{1}{3} f_i H_i r_i \Delta_i(r_i) . \quad (17)$$

For simplicity, we will assume an *Einstein-de Sitter* (EdS) universe with $\Omega_m = 1$ and $f = 1$ ($f \simeq \Omega_m^{0.55}$). Equation (16) evaluated at the initial time then yields

$$2K = (r_i H_i)^2 \left[\left(1 - \frac{\Delta_i}{3} \right)^2 - 1 - \Delta_i \right] \simeq -\frac{5}{3} (r_i H_i)^2 \Delta_i , \quad (18)$$

to linear order in $\Delta_i \ll 1$. Mass conservation then allows us to relate initial and final density contrasts following equation (11),

$$1 + \Delta = (1 + \Delta_i) \frac{r_i^3 \bar{\rho}_i}{r^3 \bar{\rho}}, \quad (19)$$

and equation (15) with $\Omega_m = 1$ gives

$$\frac{\bar{\rho}_i}{\bar{\rho}} = \left(\frac{H_i}{H} \right)^2. \quad (20)$$

Rearranging equation (16) with these identities finally yields

$$\left(\frac{\dot{r}}{r} \right)^2 = H_i^2 \left[(1 + \Delta_i) \left(\frac{r}{r_i} \right)^{-3} - \frac{5}{3} \Delta_i \left(\frac{r}{r_i} \right)^{-2} \right], \quad (21)$$

which resembles the first *Friedmann equation* of a (generally curved) matter-dominated universe with $\Omega_{m,i} = 1 + \Delta_i$ and $\Omega_{k,i} = -\frac{5}{3}\Delta_i$. In fact, for $\Delta_i = 0$ we recover the Friedmann equation of the EdS universe,

$$\left(\frac{\dot{r}}{r} \right)^2 = H_i^2 \left(\frac{r}{r_i} \right)^{-3}, \quad (22)$$

which is explicitly solved by

$$\frac{r}{r_i} = \left(\frac{3}{2} H_i t \right)^{2/3} = \left(\frac{H}{H_i} \right)^{-2/3}, \quad (23)$$

with $H = 2/3t$. However, for $\Delta_i \neq 0$ the solution can only be stated in parametric form

$$\frac{r}{r_i} = \frac{1}{2} \left(\frac{5}{3} \Delta_i \right)^{-1} (1 - \cos \eta), \quad (24)$$

$$H_i t = \frac{1}{2} \left(\frac{5}{3} \Delta_i \right)^{-3/2} (\eta - \sin \eta), \quad (25)$$

where the parameter η is defined via

$$d\eta = \frac{r_i}{r} \sqrt{\frac{5}{3}} \Delta_i H_i dt . \quad (26)$$

In particular, η becomes imaginary for $\Delta_i < 0$, and we can write

$$\frac{r}{r_i} = \frac{1}{2} \left(\frac{5}{3} |\Delta_i| \right)^{-1} (\cosh \eta - 1) , \quad (27)$$

$$H_i t = \frac{1}{2} \left(\frac{5}{3} |\Delta_i| \right)^{-3/2} (\sinh \eta - \eta) . \quad (28)$$

The simple substitutions $\Delta_i \leftrightarrow -|\Delta_i|$ and $\eta \leftrightarrow i\eta$ transform equations (24,25) and (27,28) into each other (note that $\cos(iz) = \cosh z$ and $\sin(iz) = i \sinh z$).

1.2.1 Overdensity

Let us first recap the collapse of an overdensity with $\Delta_i > 0$ [Gunn and Gott (1972)]. It decouples from the Hubble flow and starts to decrease its size after $\dot{r} = 0$, the so-called moment of *turnaround*. Equation (21) then yields

$$1 + \Delta_i = \frac{5}{3} \Delta_i \frac{r}{r_i} = \frac{1}{2} (1 - \cos \eta_{\text{ta}}) , \quad (29)$$

and for $\Delta_i \ll 1$ the turnaround parameter is $\eta_{\text{ta}} \simeq \pi$. The average density contrast evolves in time, not only because its total density ρ increases, but also because the background density of the universe $\bar{\rho}$ decreases,

$$1 + \Delta = (1 + \Delta_i) \left(\frac{r}{r_i} \right)^{-3} \left(\frac{a}{a_i} \right)^3 = (1 + \Delta_i) \frac{\left(\frac{3}{2} H_i t \right)^2}{\left[\frac{1}{2} \left(\frac{5}{3} \Delta_i \right)^{-1} (1 - \cos \eta) \right]^3} . \quad (30)$$

The time t can be related to η via equation (25), which gives

$$1 + \Delta = (1 + \Delta_i) \frac{9(\eta - \sin \eta)^2}{2(1 - \cos \eta)^3} , \quad (31)$$

and at the time of turnaround with $\eta_{\text{ta}} = \pi$

$$1 + \Delta_{\text{ta}} = (1 + \Delta_i) \frac{9\pi^2}{2^4} = (1 + \Delta_i) \left(\frac{3\pi}{4} \right)^2 \simeq 5.552. \quad (32)$$

This means, compared to its initial size, the comoving radius of the overdensity has shrunk by a factor of $(1 + \Delta_{\text{ta}})^{1/3} \simeq 1.771$. If we were to expand equation (31) to first order,

$$1 + \Delta \simeq (1 + \Delta_i) \left(1 + \frac{3}{20} \eta^2 \right), \quad (33)$$

and similarly equation (25),

$$H_i t \simeq \frac{1}{2} \left(\frac{5}{3} \Delta_i \right)^{-3/2} \frac{\eta^3}{6}, \quad (34)$$

we would obtain the following relation,

$$1 + \Delta \simeq (1 + \Delta_i) \left[1 + \Delta_i \left(\frac{3}{2} H_i t \right)^{2/3} \right]. \quad (35)$$

This demonstrates that the density perturbations initially grow at the same rate as the universe expands, see equation (23). At the time of turnaround,

$$t_{\text{ta}} = \frac{1}{2H_i} \left(\frac{5}{3} \Delta_i \right)^{-3/2} \pi, \quad (36)$$

the linear calculation yields

$$1 + \Delta_{\text{ta}} \simeq (1 + \Delta_i) \left[1 + \frac{3}{5} \left(\frac{3\pi}{4} \right)^{2/3} \right] \simeq 1 + 1.062, \quad (37)$$

where the value $\delta_{\text{ta}} \equiv 1.062$ is known as the linear density threshold for turnaround. Finally, at $\eta_c = 2\pi$, the overdensity collapses into a single point and equation (31) becomes infinite. The linear average density contrast at

time $t_c = 2t_{\text{ta}}$ then yields

$$1 + \Delta_c \simeq (1 + \Delta_i) \left[1 + \frac{3}{5} \left(\frac{6\pi}{4} \right)^{2/3} \right] \simeq 1 + 1.686, \quad (38)$$

and the value $\delta_c \equiv 1.686$ is known as the linear density threshold for collapse. Before this happens, however, shells of different r_i cross each other and eventually reach an equilibrium via virialization to form a halo. The *virial theorem* states that the average kinetic energy of the system equals minus one half its average potential energy, and thus

$$\frac{1}{2} \dot{r}_{\text{vir}}^2 \simeq \frac{1}{2} \frac{GM(r_{\text{vir}})}{r_{\text{vir}}}. \quad (39)$$

In equation (13) this yields

$$K = -\frac{1}{2} \frac{GM(r_{\text{vir}})}{r_{\text{vir}}}. \quad (40)$$

The same equation evaluated at turnaround with $\dot{r}_{\text{ta}} = 0$ gives

$$K = -\frac{GM(r_{\text{ta}})}{r_{\text{ta}}}, \quad (41)$$

leading to the conclusion that $r_{\text{vir}} = r_{\text{ta}}/2$, and thus with equation (24) to

$$\frac{1 - \cos \eta_{\text{vir}}}{1 - \cos \eta_{\text{ta}}} = \frac{1}{2}. \quad (42)$$

This requires $\eta_{\text{vir}} = 3\pi/2$ (note that $\eta_{\text{vir}} > \eta_{\text{ta}}$), and with equation (31)

$$1 + \Delta_{\text{vir}} = (1 + \Delta_i) \frac{9}{2} \left(\frac{3\pi}{2} + 1 \right)^2 \simeq 147, \quad (43)$$

at the time of virialization. After that the density of the perturbation remains constant, but the background density continues to drop. Once the full

nonlinear stage at $\eta_c = 2\pi$ has been reached, the density contrast becomes

$$1 + \Delta_c = (1 + \Delta_{\text{vir}}) \left(\frac{a_c}{a_{\text{vir}}} \right)^3 = (1 + \Delta_i) \frac{9}{2} (2\pi)^2 \simeq 178, \quad (44)$$

and its comoving size has decreased by a factor of $(1 + \Delta_c)^{1/3} \simeq 5.622$ from its initial value.

1.2.2 Underdensity

Let us now consider the case $\Delta_i < 0$ [Bertschinger (1985); Blumenthal et al. (1992)]. The evolution of an underdensity never reaches turnaround and continues to expand forever, unless $\Delta_i > 0$ on some larger scale (void-in-cloud scenario). The moment when shells of different initial radius r_i cross each other marks a stage of nonlinearity that can be interpreted as the formation of a void. In that case the infinitesimal distance between shells vanishes in one instant of time, $dr = dt = 0$. According to equation (27) we have

$$dr = \frac{1}{2} \left(\frac{5}{3} |\Delta_i| \right)^{-1} \left[(\cosh \eta - 1) \left(dr_i - r_i \frac{d\Delta_i}{\Delta_i} \right) + r_i \sinh \eta d\eta \right], \quad (45)$$

and from equation (28) we obtain

$$dt = \frac{1}{2H_i} \left(\frac{5}{3} |\Delta_i| \right)^{-3/2} \left[(\cosh \eta - 1) d\eta - \frac{3}{2} (\sinh \eta - \eta) \frac{d\Delta_i}{\Delta_i} \right]. \quad (46)$$

Setting $dt = 0$ yields

$$d\eta = \frac{3(\sinh \eta - \eta)}{2(\cosh \eta - 1)} \frac{d\Delta_i}{\Delta_i}, \quad (47)$$

which can be plugged into equation (45), and in setting $dr = 0$ this gives

$$(\cosh \eta - 1) \left(dr_i - r_i \frac{d\Delta_i}{\Delta_i} \right) + r_i \sinh \eta \frac{3(\sinh \eta - \eta)}{2(\cosh \eta - 1)} \frac{d\Delta_i}{\Delta_i} = 0, \quad (48)$$

or equivalently

$$\frac{d \ln \Delta_i}{d \ln r_i} \left[1 - \frac{3 \sinh \eta (\sinh \eta - \eta)}{2 (\cosh \eta - 1)^2} \right] = 1. \quad (49)$$

Obviously, the shell-crossing condition depends on the slope of the initial underdensity profile. From the definition of Δ in equation (10) we can derive

$$\frac{d\ln \Delta}{d\ln r} = 3 \left(\frac{\delta(r)}{\Delta(r)} - 1 \right). \quad (50)$$

For example, in the case of an inverted top-hat density distribution with

$$\delta_i(r_i) = \begin{cases} \delta_0 & \text{for } r_i < r_0 \\ 0 & \text{for } r_i \geq r_0 \end{cases}, \quad \Delta_i(r_i) = \begin{cases} \delta_0 & \text{for } r_i < r_0 \\ \delta_0 (r_0/r_i)^3 & \text{for } r_i \geq r_0 \end{cases}, \quad (51)$$

of size $r_0 > 0$ and density contrast $\delta_0 < 0$, we have

$$\frac{d\ln \Delta_i}{d\ln r_i} = \begin{cases} 0 & \text{for } r_i < r_0 \\ -3 & \text{for } r_i \geq r_0 \end{cases}. \quad (52)$$

For the case $r_i < r_0$ equation (49) only admits the trivial solution $\eta = 0$. However, for $r_i \geq r_0$ we arrive at

$$\frac{\sinh \eta (\sinh \eta - \eta)}{(\cosh \eta - 1)^2} = \frac{8}{9}, \quad (53)$$

which has the solution $\eta_{\text{sc}} \simeq 3.488$. This condition is first satisfied for the boundary shell at $r_i = r_0$, because it has the largest value of $|\Delta_i|$ at $r_i \geq r_0$, but shells of larger size successively continue to cross thereafter. We can compute the shell velocity by simply taking the derivative of equation (27) with respect to time,

$$v \equiv \frac{dr}{dt} = \frac{r_i}{2} \left(\frac{5}{3} |\Delta_i| \right)^{-1} \sinh \eta \frac{d\eta}{dt}. \quad (54)$$

From equation (28) we get

$$\frac{dt}{d\eta} = \frac{1}{2H_i} \left(\frac{5}{3} |\Delta_i| \right)^{-3/2} (\cosh \eta - 1), \quad (55)$$

so together

$$v = r_i H_i \left(\frac{5}{3} |\Delta_i| \right)^{1/2} \frac{\sinh \eta}{\cosh \eta - 1} . \quad (56)$$

Replacing r_i and H_i by their dependence on r , t , and η via equations (27,28), and using $H = 2/3t$, we arrive at

$$v = rH \frac{3 \sinh \eta (\sinh \eta - \eta)}{2 (\cosh \eta - 1)^2} . \quad (57)$$

At the moment of shell crossing, with equation (53) the velocity becomes

$$v_{\text{sc}} = \frac{4}{3} rH , \quad (58)$$

which means that the shell is moving with a peculiar velocity of $v_{\text{pec}} = v_{\text{H}}/3$ on top of the Hubble flow $v_{\text{H}} = rH$. In analogy to equation (31), the average density contrast inside the underdensity can be calculated as

$$1 + \Delta = (1 + \Delta_i) \frac{9(\sinh \eta - \eta)^2}{2(\cosh \eta - 1)^3} , \quad (59)$$

which for the shell-crossing condition $\eta_{\text{sc}} \simeq 3.488$ of the top hat yields

$$1 + \Delta_{\text{sc}} \simeq 0.2047 , \quad (60)$$

and thus $\delta_{0,\text{sc}} \simeq -0.8$. Compared to its initial size, the comoving radius of the top hat has then expanded by a factor of $(1 + \Delta_{\text{sc}})^{-1/3} \simeq 1.697$. Using equation (35) to compute the linear approximation for the average density contrast yields

$$1 + \Delta \simeq (1 + \Delta_i) \left[1 - |\Delta_i| \left(\frac{3}{2} H_i t \right)^{2/3} \right] = (1 + \Delta_i) \left[1 - \frac{3}{20} 6^{2/3} (\sinh \eta - \eta)^{2/3} \right] \quad (61)$$

Evaluated at shell crossing this results in

$$1 + \Delta_{\text{sc}} \simeq 1 - 2.717 . \quad (62)$$

The corresponding density contrast inside the top hat is known as the linear density threshold for void formation, $\delta_v \equiv -2.717$. Due to the linear extrapolation, this corresponds to an unphysical negative density, but it is nevertheless an important quantity in the excursion set theory for voids.

The derivation of δ_v relies on the assumption of an inverted top-hat density profile, which does not represent a realistic initial underdensity. One can demonstrate numerically that the density profiles around minima in a Gaussian random field [Bardeen et al. (1986)] evolve similarly, and develop a top-hat-like configuration by the time of shell crossing [Sheth and van de Weygaert (2004)]. However, the final density contrast becomes more negative in the center and the void radius stretches a bit less, as apparent from figure 1. A useful relation between linear and nonlinear underdensities inside voids is given by the approximation

$$\delta_v \simeq C [1 - (1 + \delta_{0,sc})^{-1/C}] , \quad (63)$$

with $C \simeq 1.594$ [Bernardeau (1994)]. Observationally we can only identify

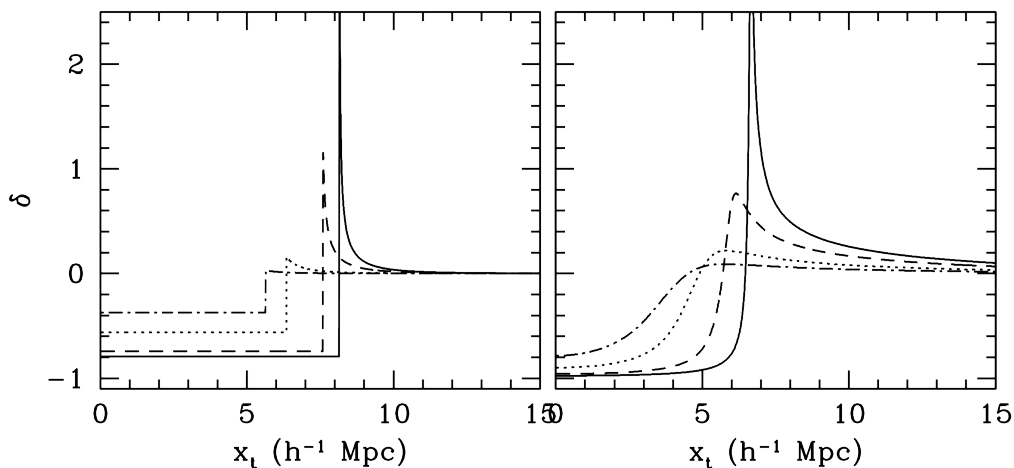


Figure 1: Void evolution from two different initial density profiles, the left panel shows a top-hat profile, the right panel the average profile around minima in a Gaussian random field. Initial average density contrast, initial characteristic radius, and subsequent time steps are identical in both cases. Adopted from Sheth and van de Weygaert (2004).

voids in the distribution of tracers of the density field, such as galaxies. The density contrast of tracers is modified by the tracer bias, which can be expressed as a multiplicative constant in the linear regime, $\delta_t = b\delta$, which represents a good approximation in void environments [Pollina et al. (2017)]. It can be used in equation (63) to calculate the linear void formation threshold in the tracer distribution [Ronconi and Marulli (2017)].

We may relax the assumption of an EdS universe and consider more general cosmologies with curvature and cosmological constant Λ . The equation of motion (13) can be extended to accommodate this [Lahav et al. (1991)],

$$\frac{1}{2}\dot{r}^2 - \frac{GM(r)}{r} - \frac{1}{6}\Lambda r^2 = K , \quad (64)$$

and the density thresholds can be expressed as functions of Ω_m [Eke et al. (1996); Lacey and Cole (1993)]. For example, in a Λ CDM cosmology with $\Omega_{m,0} \simeq 0.3$ their values become $\delta_c \simeq 1.674$ and $\delta_v \simeq -2.731$ [Jennings et al. (2013)], so their cosmology dependence is very weak.

Finally, realistic voids are neither spherical, nor isolated objects. Voids dominate the volume fraction of the cosmic web, so while expanding they are always running into their neighbors, which leads to void merging and collapse. Furthermore, voids exhibit a hierarchy of sub-voids, which has also been neglected so far. A full treatment of these properties requires sophisticated N -body simulations.

2 Excursion set theory

The aim of excursion set theory is to predict the abundance of nonlinear objects, such as halos and voids, in the cosmic density field $\rho(\mathbf{x}, t)$ at comoving coordinate \mathbf{x} and time t . For collisionless matter the density field exhibits fluctuations on arbitrarily small scales, which makes analytical calculations unfeasible. However, we can ignore fluctuations below some cutoff scale R by smoothing it with a window function W_R . Given the definition of the density contrast in equation (1), the smoothed density contrast is defined as

$$\delta_R(\mathbf{x}) = \int \delta(\mathbf{x}') W_R(\mathbf{x} - \mathbf{x}') d^3x' . \quad (65)$$

There are various choices of window functions available. The most common one is the top-hat window in real space,

$$W_R(\mathbf{x}) = \begin{cases} \frac{3}{4\pi R^3} & \text{for } |\mathbf{x}| < R \\ 0 & \text{for } |\mathbf{x}| \geq R \end{cases} . \quad (66)$$

The window is normalized such that $\int W_R(\mathbf{x}) d^3x = 1$ and has a volume of $V_R = \frac{4\pi}{3} R^3$. The Fourier transform of this window function is

$$W_R(\mathbf{k}) = \frac{3}{(kR)^3} [\sin(kR) - kR \cos(kR)] , \quad (67)$$

where \mathbf{k} is the corresponding wave vector with wavenumber k . Another option is a Gaussian window in real space,

$$W_R(\mathbf{x}) = \frac{1}{(2\pi)^{3/2} R^3} \exp\left(-\frac{x^2}{2R^2}\right) , \quad (68)$$

or a Gaussian in Fourier space,

$$W_R(\mathbf{k}) = \exp\left(-\frac{k^2 R^2}{2}\right) , \quad (69)$$

with a volume of $V_R = (2\pi)^{3/2}R^3$. These two windows are also Fourier transforms of each other. Finally, one may also consider a top-hat window in Fourier space,

$$W_R(\mathbf{k}) = \begin{cases} 1 & \text{for } |\mathbf{k}| < 1/R \\ 0 & \text{for } |\mathbf{k}| \geq 1/R \end{cases}, \quad (70)$$

with a Fourier transform of

$$W_R(\mathbf{x}) = \frac{1}{2\pi^2 R^3} \left(\frac{x}{R}\right)^{-3} \left[\sin\left(\frac{x}{R}\right) - \frac{x}{R} \cos\left(\frac{x}{R}\right) \right]. \quad (71)$$

However, note that in this case the volume is not well defined, as $\int W_R(\mathbf{x}) d^3x$ does not exist.

Equation (65) can now be evaluated with one of these window functions. This calculation is much simpler in Fourier space, where a convolution turns into a plain multiplication,

$$\delta_R(\mathbf{k}) = \delta(\mathbf{k})W_R(\mathbf{k}), \quad (72)$$

and the Fourier transform of the density contrast is given by

$$\delta(\mathbf{k}) = \int \delta(\mathbf{x}) \exp(-i\mathbf{k} \cdot \mathbf{x}) d^3x. \quad (73)$$

The joint ensemble average of the density contrast at two different locations in space defines the two-point correlation function

$$\xi(r) \equiv \langle \delta(\mathbf{x})\delta(\mathbf{x} + \mathbf{r}) \rangle, \quad (74)$$

which only depends on $r = |\mathbf{r}|$ due to statistical homogeneity and isotropy. In Fourier space we can compute a similar quantity,

$$\langle \delta(\mathbf{k})\delta(\mathbf{k}') \rangle = \iint \langle \delta(\mathbf{x})\delta(\mathbf{x}') \rangle \exp(-i\mathbf{k} \cdot \mathbf{x}) \exp(-i\mathbf{k}' \cdot \mathbf{x}') d^3x d^3x', \quad (75)$$

and choosing $\mathbf{x}' = \mathbf{x} + \mathbf{r}$ it can be rearranged to

$$\begin{aligned} \langle \delta(\mathbf{k})\delta(\mathbf{k}') \rangle &= \iint \langle \delta(\mathbf{x})\delta(\mathbf{x}+\mathbf{r}) \rangle \exp[-i(\mathbf{k} + \mathbf{k}') \cdot \mathbf{x}] \exp(-i\mathbf{k}' \cdot \mathbf{r}) \, d^3x \, d^3r = \\ &= \int \xi(r) \exp(-i\mathbf{k}' \cdot \mathbf{r}) \, d^3r \int \exp[-i(\mathbf{k} + \mathbf{k}') \cdot \mathbf{x}] \, d^3x \equiv P(\mathbf{k}')(2\pi)^3 \delta_D(\mathbf{k}+\mathbf{k}') \end{aligned} \quad (76)$$

The latter equality defines the power spectrum as a Fourier transform of the correlation function,

$$P(k) = \int \xi(r) \exp(-i\mathbf{k} \cdot \mathbf{r}) \, d^3r, \quad (77)$$

which likewise merely depends on the magnitude of \mathbf{k} . We can now define the variance of the density field as

$$\sigma_R^2 \equiv \langle \delta_R^2(\mathbf{x}) \rangle = \xi_R(r=0) = \frac{1}{(2\pi)^3} \int P_R(k) \, d^3k = \frac{1}{2\pi^2} \int P(k) W_R^2(k) k^2 \, dk. \quad (78)$$

For example, considering a simple power law with $P(k) \propto k^n$ and a Fourier space top-hat window,

$$\sigma_R^2 \propto \int_0^\infty P(k) W_R^2(k) k^2 \, dk \propto \int_0^{1/R} k^{n+2} \, dk \propto R^{-n-3}. \quad (79)$$

If we associate a mass $M = \frac{4\pi}{3} R^3 \bar{\rho}$ to regions of size R , we have

$$\sigma_R^2 \propto M^{-n/3-1}. \quad (80)$$

As long as $n > -3$, σ_R^2 is a decreasing function of M , i.e. smaller objects originate from larger density fluctuations and therefore form at earlier times. This corresponds to the so-called *hierarchical clustering scenario*.

2.1 Overdensity

Now let us assume that the smoothed density contrast δ_R initially is a Gaussian random field with probability distribution function

$$p(\delta_R) = \frac{1}{\sqrt{2\pi}\sigma_R} \exp\left(-\frac{\delta_R^2}{2\sigma_R^2}\right), \quad (81)$$

and that above some critical density threshold the matter inside regions of scale R start to collapse. We may pick $\delta_c = 1.686$ for this threshold as motivated above. The total fraction of collapsed objects of size R or larger is then calculated as [Press and Schechter (1974)]

$$F(\sigma_R, \delta_c) = \int_{\delta_c}^{\infty} p(\delta_R) d\delta_R = \frac{1}{2} \operatorname{erfc}\left(\frac{\nu}{\sqrt{2}}\right), \quad (82)$$

where erfc denotes the complimentary error function and $\nu \equiv \delta_c/\sigma_R$. Note that $F(R \rightarrow 0, \delta_c) = F(\sigma_R \rightarrow \infty, \delta_c) = 1/2$, so this calculation seems to disregard one half of all collapsed objects. In order to resolve this apparent paradox, let us consider a sequence in δ_R when R is decreased stepwise from a large initial value. According to equation (81) and assuming a Fourier-space top-hat window, in which case the smoothed density contrasts at scale R and R' are independent for $R \neq R'$, δ_R performs a random walk as schematically depicted in figure 2. Due to symmetry, every walk that up-crosses the threshold at a given value R' has a mirror-symmetric counterpart that moves below the threshold again after $\delta_{R'} = \delta_c$. Hence, when evaluating equation (82) for the value R we have to account for all the walks that have already crossed the threshold and therefore collapsed at $R' > R$, which exactly yields a factor of two [Bond et al. (1991)].

We may also worry about walks that up-cross the threshold multiple times, but this will not affect the final number of collapsed objects, because regions collapsing inside a larger collapsing region will be subsumed by the latter and should not be counted as individual objects. This scenario is also referred to as the *cloud-in-cloud* process. The fundamental quantity to describe the number of collapsed objects of size R is therefore given by the

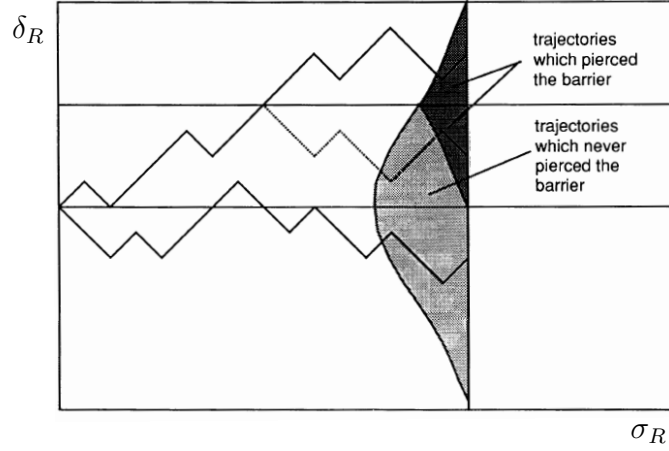


Figure 2: Schematic random walks performed by δ_R for decreasing values of R (i.e. increasing σ_R). The upper horizontal line shows the threshold barrier $\delta_R = \delta_c$, the lower line $\delta_R = 0$. Adopted from [Bond et al. \(1991\)](#).

first-crossing distribution

$$f(\sigma_R, \delta_c) \equiv \frac{dF}{d\sigma_R^2} = \frac{\delta_c}{\sqrt{2\pi}\sigma_R^3} \exp\left(-\frac{\delta_c^2}{2\sigma_R^2}\right), \quad (83)$$

a detailed derivation of which is presented in [Zentner \(2007\)](#). It can directly be related to the number density n of halos with via $dn = \frac{\bar{\rho}}{M}|dF|$ and thus

$$\frac{dn}{dM} = \frac{\bar{\rho}}{M} f(\sigma_R, \delta_c) \left| \frac{d\sigma_R^2}{dM} \right|, \quad (84)$$

where dn/dM is the halo mass function, stating the number density of halos with masses between M and $M+dM$. Expressing this in terms of the variable $\nu = \delta_c/\sigma_R$ and noting that

$$d \ln \sigma_R^2 = \frac{d\sigma_R^2}{\sigma_R^2} = \frac{1}{\sigma_R^2} d\left(\frac{\delta_c^2}{\nu^2}\right) = -\frac{2}{\sigma_R^2} \frac{\delta_c^2}{\nu^3} d\nu = -2 \frac{d\nu}{\nu} = -2 d \ln \nu, \quad (85)$$

we arrive at

$$\frac{dn}{dM} = \frac{\bar{\rho}}{M^2} \sigma_R^2 f(\sigma_R, \delta_c) \left| \frac{d \ln \sigma_R^2}{d \ln M} \right| = \frac{\bar{\rho}}{M^2} \nu f(\nu) \frac{d \ln \nu}{d \ln M}, \quad (86)$$

with

$$\nu f(\nu) = \sqrt{\frac{2}{\pi}} \nu \exp\left(-\frac{\nu^2}{2}\right). \quad (87)$$

The functional form of this expression is independent of cosmology, unlike σ_R , so it is referred to as a *universal* halo mass function.

2.2 Underdensity

In order to define the abundance of voids, one may simply exchange the overdense threshold δ_c by the underdensity δ_v in the formalism above. This is accurate initially, but subsequent gravitational evolution destroys the symmetry. Consider a random walk that up-crosses δ_c at some scale R and then down-crosses δ_v at scale $R' < R$. This corresponds to a void embedded in a larger-scale overdensity that is bound to collapse, which means that the void is doomed to be squeezed out of existence. The latter phenomenon is known as the *void-in-cloud* process. Analogously one can also define the *void-in-void* process, which is responsible for the formation of sub-voids, the *cloud-in-void* process, and the *cloud-in-cloud* process already discussed above. The random-walk trajectories for the four cases are exemplified in figure 3, along with their corresponding regions in an N -body simulation.

In order to isolate the surviving voids, we have to modify equation (83) by subtracting all voids that are affected by the void-in-cloud process,

$$f(\sigma_R, \delta_v, \delta_c) = f(\sigma_R, \delta_v) - \int_0^{\sigma_R^2} f(\sigma_{R'}, \delta_c) f(\sigma_R, \delta_v | \sigma_{R'}, \delta_c) d\sigma_{R'}^2. \quad (88)$$

That is, the number of voids of size R is determined by the fraction of walks that cross the threshold δ_v at R , minus the fraction of those that had crossed δ_c at all $R' > R$ before reaching δ_v . The latter term is a product of the fraction of all walks that cross δ_c at R' times the fraction of walks that cross δ_v at R , if they have already crossed δ_c at R' , which needs to be integrated over all R' . The solution of equation (88) can be found with the help of

Laplace transforms, as shown in Sheth and van de Weygaert (2004),

$$f(\sigma_R, \delta_v, \delta_c) = \sum_{j=1}^{\infty} \frac{j^2 \pi^2 D^2}{\delta_v^2} \frac{\sin(j\pi D)}{j\pi} \exp\left(-\frac{j^2 \pi^2 D^2}{2\delta_v^2 / \sigma_R^2}\right). \quad (89)$$

The variable D is the so-called *void-and-cloud* parameter, defined as

$$D \equiv \frac{|\delta_v|}{\delta_c + |\delta_v|}. \quad (90)$$

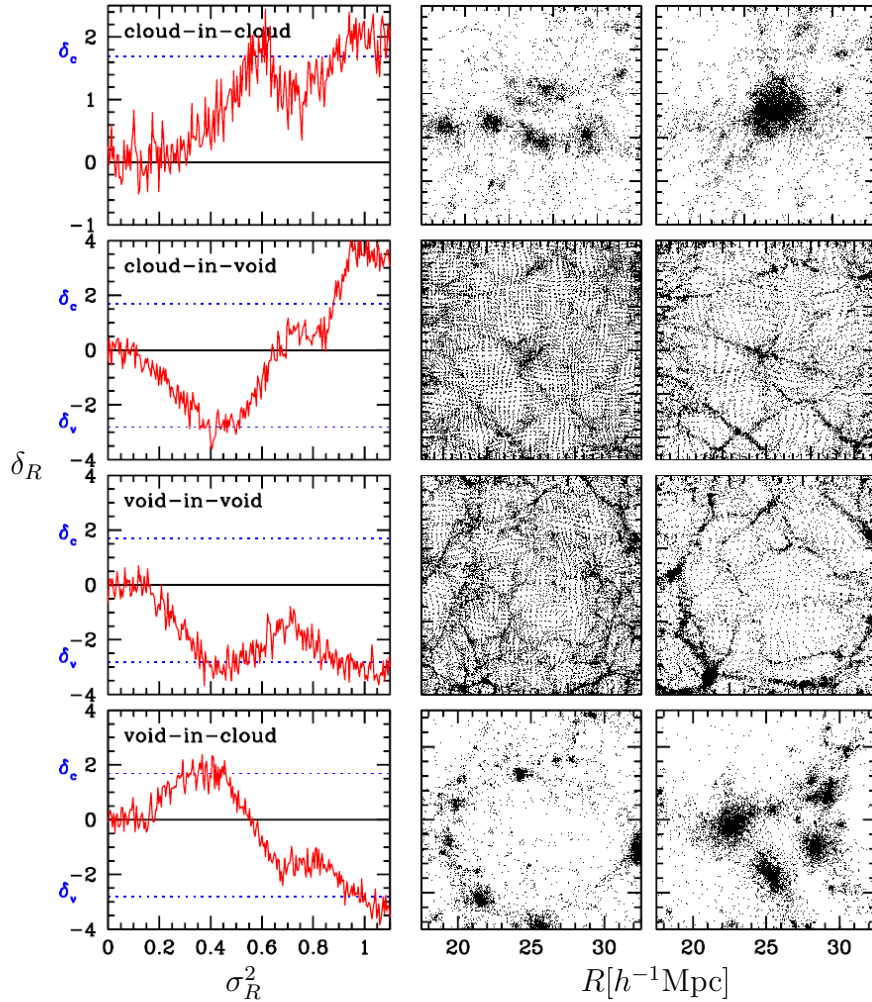


Figure 3: Random walks performed by δ_R in four distinct cases. The right panels show the associated evolution of the particle distribution in an N -body simulation. Adopted from Sheth and van de Weygaert (2004).

It determines the importance of the void-in-cloud process via the relative difference between the values of δ_c and δ_v . For example, the total mass fraction inside voids is given by

$$\int f(\sigma_R, \delta_v, \delta_c) d\sigma_R^2 = 1 - D = \frac{\delta_c}{\delta_c + |\delta_v|}. \quad (91)$$

For $\delta_c \gg |\delta_v|$, D is small and voids account for nearly all the mass in the universe. On the other hand, if $\delta_c \ll |\delta_v|$, almost all the mass is bound inside halos. Equation (89) can be converted into a simpler approximative form for $\delta_c/|\delta_v| \gtrsim 1/4$ [Sheth and van de Weygaert (2004)],

$$\nu f(\nu) \simeq \sqrt{\frac{2}{\pi}} \nu \exp\left(-\frac{\nu^2}{2}\right) \exp\left[-\frac{|\delta_v|}{\delta_c} \left(\frac{D}{2\nu}\right)^2 - 2\left(\frac{D}{\nu}\right)^4\right], \quad (92)$$

with $\nu = |\delta_v|/\sigma_R$. The first part coincides with equation (83), and the second one is responsible for the void-in-cloud process. The two exponentials quickly decay at very low and high ν , so the void distribution is peaked around values of $\nu \simeq 1$, as depicted in figure 4 for three different values of δ_c . δ_c mostly affects small voids via the void-in-cloud process, but the abundance of large voids is dictated by the value of δ_v only.

The typical comoving size of voids can be roughly estimated with the help of equation (79) stating $\sigma_R^2 \propto R^{-n-3}$. For $\nu \simeq 1$ we have $\sigma_R \simeq |\delta_v|$ and therefore

$$R \simeq 8h^{-1}\text{Mpc} \left(\frac{\sigma_8}{|\delta_v|}\right)^{\frac{2}{n+3}}, \quad (93)$$

which corresponds to the size of the excursion-set region when it crosses the threshold δ_v . After that the void expands nonlinearly and, according to spherical evolution, stretches by a factor of 1.697 until shell crossing. Assuming $\sigma_8 = 0.83$, $|\delta_v| = 2.717$, and $n = -1.5$ we then obtain $R_v \simeq 3h^{-1}\text{Mpc}$. In analogy to equation (84) we can define a void mass function. However, a more natural quantity to describe voids is their volume V_v , or their effective radius

$$R_v \equiv \left(\frac{3}{4\pi}V_v\right)^{1/3}. \quad (94)$$

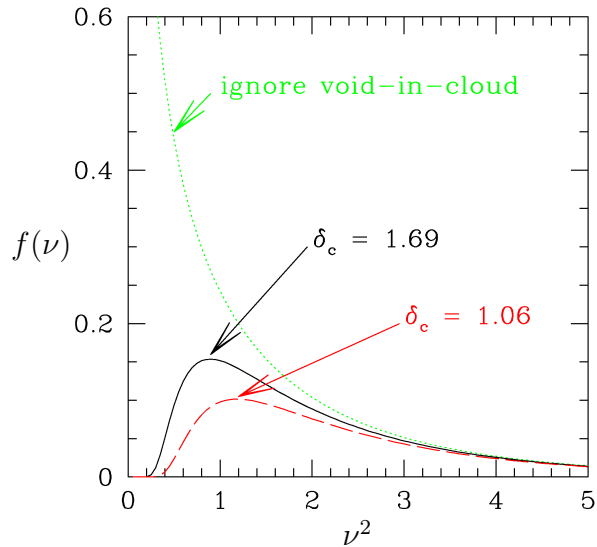


Figure 4: Three versions of equation (92) with $\delta_c = 1.06$ (dashed), $\delta_c = 1.69$ (solid), and $\delta_c \rightarrow \infty$ (dotted). In each case, $\delta_v = -2.81$. Adopted from Sheth and van de Weygaert (2004).

The comoving volume of a void can be related to its mass M and initial excursion-set scale R via

$$V_v = \frac{M}{\bar{\rho}} \left(\frac{R_v}{R} \right)^3, \quad (95)$$

where the ratio $R_v/R \simeq 1.697$ is given by spherical evolution. Now equation (86) can be rewritten in terms of

$$dM = \left(\frac{R}{R_v} \right)^3 \bar{\rho} dV_v = \left(\frac{R}{R_v} \right)^3 \bar{\rho} 4\pi R_v^2 dR_v = 3M \, d\ln R_v, \quad (96)$$

and $d\ln M = 3 \, d\ln R_v$, which yields the void size function

$$\frac{dn}{d\ln R_v} = \frac{1}{V_v} \left(\frac{R_v}{R} \right)^3 \nu f(\nu) \frac{d\ln \nu}{d\ln R_v}. \quad (97)$$

We can now determine the cumulative volume fraction of all voids larger than

a given size R_v ,

$$F_v(R_v) = \int_{R_v}^{\infty} \frac{dn}{d \ln R'_v} V_v d \ln R'_v = \left(\frac{R_v}{R} \right)^3 \int_{\nu(R_v)}^{\infty} \nu f(\nu) d \ln \nu, \quad (98)$$

which for all voids down to $R_v = 0$, with equation (91) becomes

$$F_v(0) = \left(\frac{R_v}{R} \right)^3 (1 - D). \quad (99)$$

For $\delta_v = -2.717$, $\delta_c = 1.686$, and $R_v/R = 1.697$ we obtain $F_v(0) \simeq 1.871$, which is unphysical as it exceeds unity. If we relax the shell-crossing condition by choosing a less negative value for δ_v and use equation (63) to calculate the corresponding nonlinear void stretch R_v/R , $F_v(0)$ is reduced, but at the expense of increasing the number of large voids. Only for $\delta_v \rightarrow 0$ and thus $D \rightarrow 0$ and $R_v/R \rightarrow 1$ we restore physicality with $F_v(0) = 1$. Note that in the derivation of equation (99) we have assumed the number density of voids to be conserved during nonlinear evolution. However, due to the finite amount of available volume in the universe, many voids will end up merging with each other. This argues for the total volume of voids being conserved, and not their number density [Jennings et al. (2013)]. Therefore we may require $F_v(R_v) = F_v(R)$ during nonlinear evolution, and thus

$$V_v dn(R_v) = V dn(R), \quad (100)$$

which modifies equation (97) to

$$\frac{dn(R_v)}{d \ln R_v} = \frac{V}{V_v} \frac{dn(R)}{d \ln R} \frac{d \ln R}{d \ln R_v} = \frac{1}{V_v} \nu f(\nu) \frac{d \ln \nu}{d \ln R_v}. \quad (101)$$

Here we assumed $d \ln R / d \ln R_v = 1$, which applies in the spherical evolution model, but may not hold in general. In this case the total void volume fraction becomes $F_v(0) = 1 - D$, obeying physicality for all values of δ_v and δ_c , and in particular $F_v(0) \simeq 0.383$ for $\delta_v = -2.717$ and $\delta_c = 1.686$.

3 Clustering statistics

3.1 Void profile

The void density profile is defined as the spherically averaged relative deviation of mass density around a void center from the mean value $\bar{\rho}$ across the universe,

$$u_v(r) \equiv \frac{\rho_v(r)}{\bar{\rho}} - 1. \quad (102)$$

Figure 5 shows such average density profiles from dark matter N -body simulations for voids of different size. Voids are deeply underdense in their interiors, most notably the smallest ones. The profiles all exhibit overdense compensation walls with a maximum located slightly outside their effective radius, shifting outwards for larger voids. The height of the compensation wall decreases with void size, causing the inner profile slope to become shallower and the wall to widen. This trend divides all voids into being either *overcompensated* or *undercompensated*, depending on whether the total mass within their compensation wall exceeds or falls behind their missing mass in the center, respectively. Ultimately, at sufficiently large distances to the void center, all profiles approach the mean background density. A simple empirical formula can accurately capture the properties described above,

$$u_v(r) = \delta_c \frac{1 - (r/r_s)^\alpha}{1 + (r/R_v)^\beta}, \quad (103)$$

where δ_c is the central density contrast, r_s a scale radius at which $\rho_v = \bar{\rho}$, and α and β determine the inner and outer slope of the void's compensation wall, respectively [Hamaus et al. (2014a)].

The lower panel of figure 5 depicts the corresponding radial velocity profiles. Note that a positive velocity implies outflow of tracer particles from the void center, while a negative one denotes infall. As the largest voids are undercompensated (void-in-void scenario), i.e. the total mass in their surrounding does not make up for the missing mass in their interior, they are characterized by outflows in the entire distance range. Tracer velocities increase almost linearly from the void center until they reach a maximum lo-

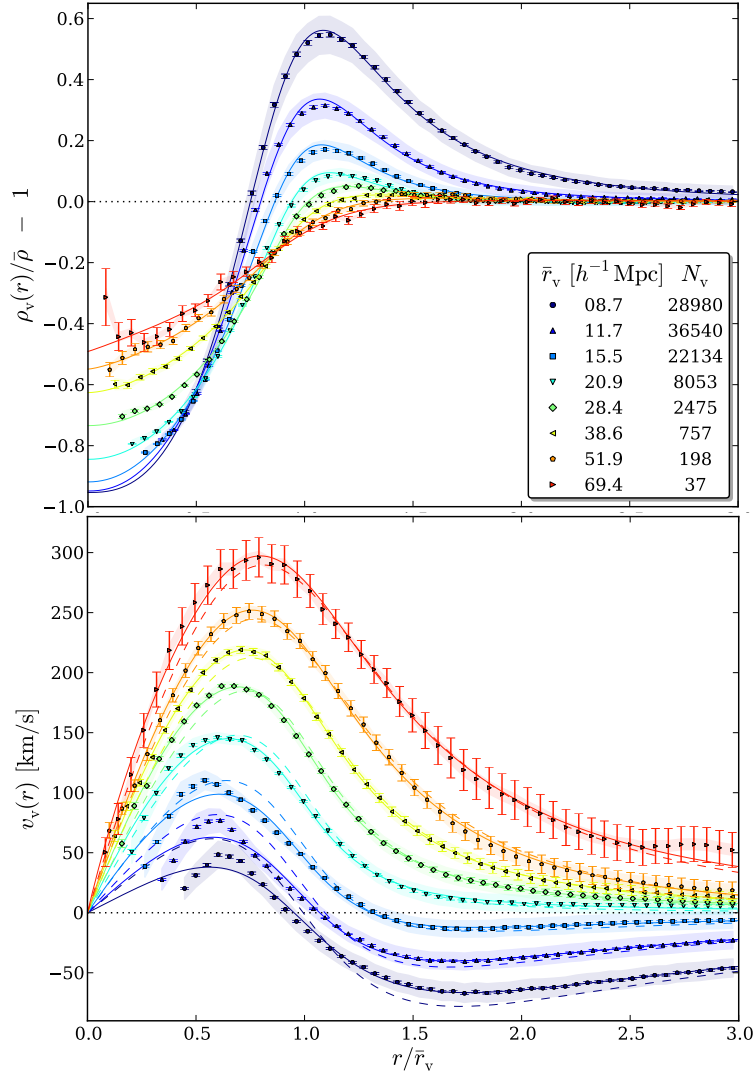


Figure 5: Density (top) and velocity (bottom) profiles of voids at redshift zero in 8 contiguous bins in void radius with mean values and void counts indicated in the inset. Solid lines represent best-fit solutions from equation (103) for density – and from equations (9) and (104) for velocity profiles. Adopted from Hamaus et al. (2014a).

cated slightly below the effective void radius of each sample, which indicates the increasing influence of the overdense compensation wall. When passing the latter, tracer velocities are continuously decreasing again in amplitude and approach zero in the large distance limit. Small voids may exhibit infall velocities, as they can be overcompensated (void-in-cloud scenario). This

causes a sign change in their velocity profile around the void's effective radius beyond which matter is flowing onto its compensation wall, ultimately leading to a collapse of the void. Moreover, because small voids are more underdense in the interior, their velocity profile is more nonlinear and less accurately sampled there. The distinction between overcompensation and undercompensation can directly be inferred from velocities, since only overcompensated voids feature a sign change in their velocity profile, while undercompensated ones do not. Consequently, the flow of tracer particles around precisely compensated voids vanishes already at a finite distance to the void center and remains zero outwards.

In linear theory the velocity profile can be related to the density profile using equations (9) and (10). With the empirical form of equation (103), the average density contrast becomes

$$\Delta(r) = \delta_c {}_2F_1\left[1, \frac{3}{\beta}, \frac{3}{\beta} + 1, -(r/R_v)^\beta\right] - \frac{3\delta_c(r/r_s)^\alpha}{\alpha + 3} {}_2F_1\left[1, \frac{\alpha + 3}{\beta}, \frac{\alpha + 3}{\beta} + 1, -(r/R_v)^\beta\right], \quad (104)$$

where ${}_2F_1$ is the Gauss hypergeometric function. When plugged into equation (9), this can be used to compare to the velocity profiles obtained from simulations, the results are shown as solid lines in the lower panel of figure 5. With the explicit form for the average density contrast in equation (104), it is straightforward to determine the void's uncompensated mass, defined as

$$\delta M = \lim_{r \rightarrow \infty} \frac{4\pi}{3} \bar{\rho} r^3 \Delta(r). \quad (105)$$

The limit exists only for $\beta > \alpha + 3$ and yields

$$\delta M = \frac{4\pi^2 \bar{\rho} R_v^3 \delta_c}{\beta} \left\{ \csc(3\pi/\beta) - (R_v/r_s)^\alpha \csc[(\alpha + 3)\pi/\beta] \right\}, \quad (106)$$

i.e., independently of δ_c , compensated voids with $\delta M = 0$ satisfy the relation

$$\left(\frac{r_s}{R_v}\right)^\alpha = \frac{\sin(3\pi/\beta)}{\sin[(\alpha + 3)\pi/\beta]}. \quad (107)$$

3.2 Void model

In analogy to the well studied *halo model* [Cooray and Sheth (2002)], we can define a *void model* of large-scale structure that similarly assumes the entire matter distribution to be described as a superposition of voids [Hamaus et al. (2014b)]. In this manner, the cross-power spectrum between void centers and halos can be split into two terms as a function of wavenumber k – a *one-void* (or *shot noise*) term

$$P_{\text{vh}}^{(1\nu)}(k) = \frac{1}{\bar{n}_{\text{v}}\bar{n}_{\text{h}}} \int \frac{dn_{\text{v}}(R_{\text{v}})}{dR_{\text{v}}} N_{\text{h}}(R_{\text{v}}) u_{\text{v}}(k|R_{\text{v}}) dR_{\text{v}}, \quad (108)$$

which only considers correlations between the N_{h} halos and the void center within any given void of radius R_{v} , and a *two-void* term responsible for correlations between halos and void centers in distinct voids,

$$P_{\text{vh}}^{(2\nu)}(k) = \frac{1}{\bar{n}_{\text{v}}\bar{n}_{\text{h}}} \iint \frac{dn_{\text{v}}(R_{\text{v}})}{dR_{\text{v}}} \frac{dn_{\text{h}}(M_{\text{h}})}{dM_{\text{h}}} b_{\text{v}}(R_{\text{v}}) b_{\text{h}}(M_{\text{h}}) \times u_{\text{v}}(k|R_{\text{v}}) P_{\text{mm}}(k) dR_{\text{v}} dM_{\text{h}}. \quad (109)$$

$dn_{\text{v}}/dR_{\text{v}}$ and $dn_{\text{h}}/dM_{\text{h}}$ are, respectively, the void size function and the halo mass function. Their corresponding linear bias parameters are b_{v} and b_{h} . $u_{\text{v}}(k|R_{\text{v}})$ describes the normalized density profile for voids of radius R_{v} in Fourier space and $P_{\text{mm}}(k)$ the auto-power spectrum of dark matter. For a narrow range in R_{v} , the total void-halo cross-power spectrum becomes

$$P_{\text{vh}}(k) \simeq b_{\text{v}} b_{\text{h}} u_{\text{v}}(k) P_{\text{mm}}(k) + \bar{n}_{\text{v}}^{-1} u_{\text{v}}(k), \quad (110)$$

where all explicit dependences on void radius and halo mass have been dropped for simplicity. Analogously, for the auto-power spectra of voids and halos the model yields

$$P_{\text{vv}}(k) \simeq b_{\text{v}}^2 P_{\text{mm}}(k) + \bar{n}_{\text{v}}^{-1}, \quad (111)$$

$$P_{\text{hh}}(k) \simeq b_{\text{h}}^2 P_{\text{mm}}(k) + \bar{n}_{\text{h}}^{-1}, \quad (112)$$

so in the high sampling limit of $\bar{n}_v^{-1}, \bar{n}_h^{-1} \ll P_{\text{mm}}$, the void density profile in Fourier space can be estimated as

$$u_v(k) \simeq \frac{b_h P_{\text{vh}}(k)}{b_v P_{\text{hh}}(k)} \simeq \frac{P_{\text{vh}}(k)}{P_{\text{hh}}(k)} \times \frac{P_{\text{hh}}(k)}{P_{\text{vh}}(k)} \Big|_{k \rightarrow 0} . \quad (113)$$

Its relation to configuration space can be expressed via

$$u_v(k) = \frac{\bar{\rho}}{\delta M} \int_0^\infty u_v(r) \frac{\sin(kr)}{kr} 4\pi r^2 dr , \quad (114)$$

where $u_v(r)$ is the density profile in configuration space and δM the void's uncompensated mass. The profile is normalized such that $u_v(k \rightarrow 0) = 1$ [Cooray and Sheth (2002)], i.e.

$$\delta M = \bar{\rho} \int_0^\infty u_v(r) 4\pi r^2 dr . \quad (115)$$

From equation (114) we also have $u_v(k \rightarrow \infty) = 0$, assuming $|ru_v(r)| < \infty$. Likewise, $u_v(r \rightarrow \infty) = 0$, as voids are local structures with a finite extent. The remaining limit is determined by the matter density in the void center, which for an empty void yields $u_v(r \rightarrow 0) = -1$.

Simulation results for the various power spectra between dark matter, mock galaxies (as observational proxies for halos), and voids are shown in figure 6. While the auto-power spectrum of galaxies closely follows the shape of the underlying matter power spectrum, this is not the case for voids. Here the shot noise term in equation (111) dominates over the bare clustering term. The latter is suppressed due to the low bias parameter of the selected voids, in this case $b_v \simeq 0.8$. The cross-power spectrum between galaxies and voids largely avoids this problem, as shot noise turns out to be much lower. We can identify two regimes as suggested by equation (110): linear clustering with constant bias on large scales and a nonlinear suppression of power on small scales due to the void profile. The cross-power spectrum even turns negative and reaches a minimum at $k \sim \pi/R_v$, a consequence of galaxy-void exclusion, which also causes the shot noise to be much lower than expected from equation (110).

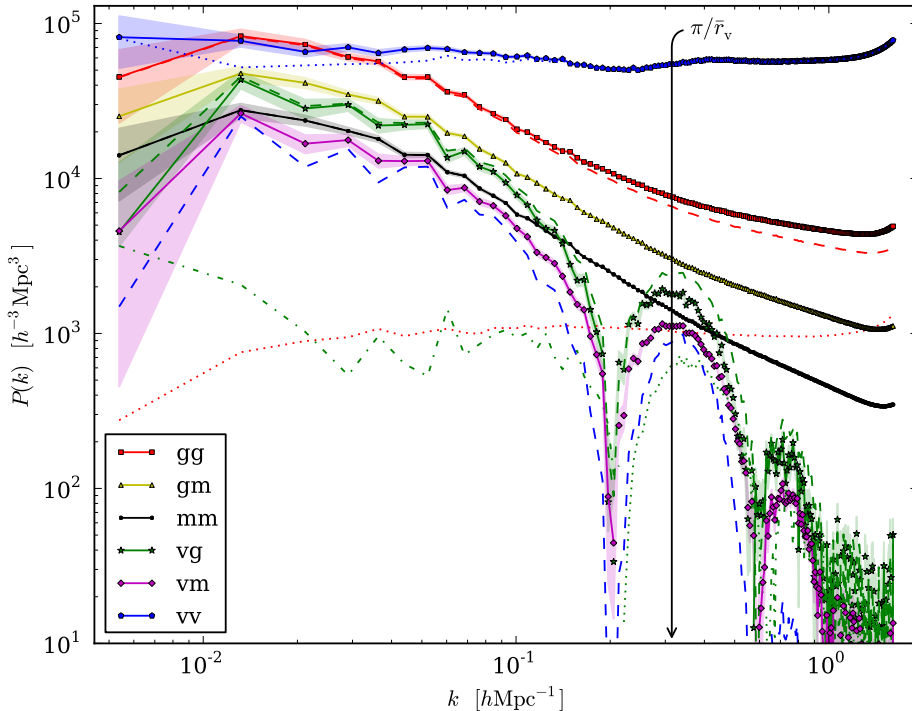


Figure 6: Auto- and cross-power spectra for all possible combinations of dark matter, galaxies and voids (solid lines connected by symbols, line omitted when negative). Subtracting shot noise (drawn in dotted if positive and dot-dashed if negative) yields the dashed lines. Shaded bands show 1σ -uncertainties. Adopted from Hamaus et al. (2014b).

For the particular case of a compensated void, whose density decrement in its center is exactly balanced by an overdense wall around it, the normalization condition $u_v(k \rightarrow 0) = 1$ cannot be enforced, as $\delta M = 0$. Due to the geometric definition of voids it is more meaningful to normalize equation (114) by the void volume V_v , which yields a renormalized profile $b_v(k)$ with

$$\frac{\delta M}{\bar{\rho} V_v} u_v(k) \equiv b_v(k), \quad (116)$$

such that $|b_v(k)| < \infty$ for all δM . This matches the large-scale clustering properties of voids in the linear regime to the nonlinear domain of the internal void structure, so it can be interpreted as a scale-dependent void bias $b_v(k) \equiv b_v u_v(k)$. In particular, it agrees with the fact that compen-

sated structures ($\delta M = 0$) do not generate any large-scale power ($b_v = 0$), because they only rearrange mass locally [Cooray and Sheth (2002)]. Equation (116) gives a simple explanation of linear bias: it is the uncompensated mass $\delta M = M - \bar{\rho}V$ of a tracer compared to the mass of an equally sized region of volume V of the background, $b = \delta M / \bar{\rho}V$. This is indeed predicted by so-called *Poisson cluster models* [Sheth (1998)], where halo bias arises as a consequence of mass conservation, or in other words: the distribution of halos depends on their environment. Thanks to the symmetry of the initial Gaussian field, this argument applies to voids just as well, with the advantage of the volume of voids being observationally more accessible than the volume of halos. Unfortunately, uncompensated mass is not directly observable (except via gravitational lensing), but we can define a similar relation to equation (116) using galaxies as tracer particles, with the replacements $\delta M \rightarrow \delta N_g = N_g - \bar{n}_g V$ and $\bar{\rho} \rightarrow \bar{n}_g$. This yields the relative bias between voids and galaxies,

$$\frac{\delta N_g}{\bar{n}_g V_v} u_v(k) \simeq \frac{b_v(k)}{b_g}. \quad (117)$$

The zero-crossing of the relative bias as a function of R_v provides the void radius of compensation. As it coincides with the zero-crossing of the absolute void bias $b_v(R_v)$, this suggests that if voids are compensated by galaxies ($\delta N_g = 0$), they are also compensated in mass ($\delta M = 0$) and vice versa. If mass conservation is assumed, only compensated voids should remain compensated in the course of cosmological evolution and may therefore serve as a *static ruler* on scales much smaller than the baryon acoustic oscillations (conversely, mass conservation can be tested on cosmological scales if compensated voids are assumed to be static rulers). In contrast to a *standard ruler* the comoving size of a static ruler is not necessarily determined by a physical scale, but it is conserved and thus can be used to probe the expansion history of the universe. In simulations, the zero-crossing of $b_v(R_v)$ is found at $R_v \simeq 20h^{-1}\text{Mpc}$, independently of redshift [Hamaus et al. (2014b)].

4 Cosmology with voids

4.1 Redshift-space distortions

Let us consider a void center at comoving coordinate \mathbf{X} located on our line of sight, and a galaxy at location \mathbf{x} , with separation $\mathbf{r} = \mathbf{x} - \mathbf{X}$ from it (unless necessary, the subscripts referring to galaxies and voids are omitted in this section). Because we use the redshift z of the galaxy to determine its comoving distance to us, its peculiar velocity \mathbf{v} will have a contribution via the Doppler effect [Kaiser (1987)], so the inferred separation between the galaxy and the void center in redshift space is

$$\mathbf{s} = \mathbf{r} + (1 + z) \frac{\hat{\mathbf{X}} \cdot \mathbf{v}}{H(z)} \hat{\mathbf{X}}, \quad (118)$$

where $H(z)$ is the Hubble rate, $\hat{\mathbf{X}} = \mathbf{X}/|\mathbf{X}|$, and we assumed $|\mathbf{r}| \ll |\mathbf{X}|$ such that \mathbf{x} and \mathbf{X} are approximately parallel (distant-observer approximation). As long as we only consider relative motions between galaxies and void centers on scales of the void extent, bulk motions between different voids can be neglected.

The galaxy's peculiar velocity is sourced by the underlying mass distribution of the void, which obeys spherical symmetry in the cosmic average. According to the linearized mass-conservation equation (9), it can be related to the average mass-density contrast $\Delta(r)$ within radius $r = |\mathbf{r}|$ around the void center,

$$\mathbf{v}(\mathbf{r}) = -\frac{1}{3} \frac{f(z)H(z)}{1+z} \mathbf{r} \Delta(r), \quad (119)$$

where $f(z)$ is the logarithmic growth rate for linear density perturbations. Assuming General Relativity (GR) and the standard Λ CDM-model for cosmology, it can be expressed as a power of the matter-density parameter, $f(z) = \Omega_m^\gamma(z)$, with a growth index of $\gamma \simeq 0.55$. The void-galaxy cross-correlation function in redshift space, ξ^s , can be related to its real-space

counterpart ξ via the general transformation

$$1 + \xi^s(\mathbf{s}) = \int [1 + \xi(r)] \mathcal{P}(\mathbf{v}, \mathbf{r}) d^3v, \quad (120)$$

where the pairwise velocity probability distribution function $\mathcal{P}(\mathbf{v}, \mathbf{r})$ maps all void-galaxy pairs of separation \mathbf{r} to separation \mathbf{s} depending on their relative velocity \mathbf{v} . According to equation (118) only the magnitude of the relative velocity component along the line of sight $v_{\parallel} \equiv \hat{\mathbf{X}} \cdot \mathbf{v}$ affects the vector \mathbf{s} , which reduces equation (120) to a one-dimensional integral via the replacements $\mathcal{P}(\mathbf{v}, \mathbf{r}) \rightarrow \mathcal{P}(v_{\parallel}, \mathbf{r})$ and $d^3v \rightarrow dv_{\parallel}$. A Gaussian form for the pairwise velocity probability distribution function in most cases provides a reasonable approximation,

$$\mathcal{P}(v_{\parallel}, \mathbf{r}) \simeq \frac{1}{\sqrt{2\pi}\sigma_v(\mathbf{r})} \exp \left[-\frac{(v_{\parallel} - v(r)\frac{r_{\parallel}}{r})^2}{2\sigma_v^2(\mathbf{r})} \right], \quad (121)$$

with a mean of $v(r)r_{\parallel}/r$, where $r_{\parallel} \equiv \hat{\mathbf{X}} \cdot \mathbf{r}$, and dispersion σ_v . This model is referred to as the *Gaussian streaming model* as a description for the galaxy auto-correlation function in redshift space [Fisher (1995)]. We can now make use of equation (119) to relate the void velocity profile to the average density contrast, which itself depends on the void density profile via equation (10). Assuming a specific form for the density profile, such as equation (103), allows to fully specify the void-galaxy cross-correlation function of equation (120) [Hamaus et al. (2016, 2015)]. Figure 7 shows this function as calculated from a large simulation of mock galaxies, including a best-fit Gaussian streaming model using equation (103) as a template for the void density profile.

Note that the real-space cross-correlation function $\xi(r)$ is nothing else than the void galaxy-density profile $u_{\text{vg}}(r)$ in this case. Labeling each of all N_v void centers with index i and coordinates \mathbf{X}_i , and similarly each of all N_g galaxies with index j and coordinates \mathbf{x}_j , we have

$$u_{\text{vg}}(r) + 1 = \frac{n_{\text{vg}}(r)}{\bar{n}_g} = \frac{1}{N_v} \sum_i \frac{n_{\text{vg}}^{(i)}(r)}{\bar{n}_g} = \frac{1}{N_v} \sum_i \frac{V}{N_g} \sum_j \delta^D(\mathbf{X}_i - \mathbf{x}_j + \mathbf{r}), \quad (122)$$

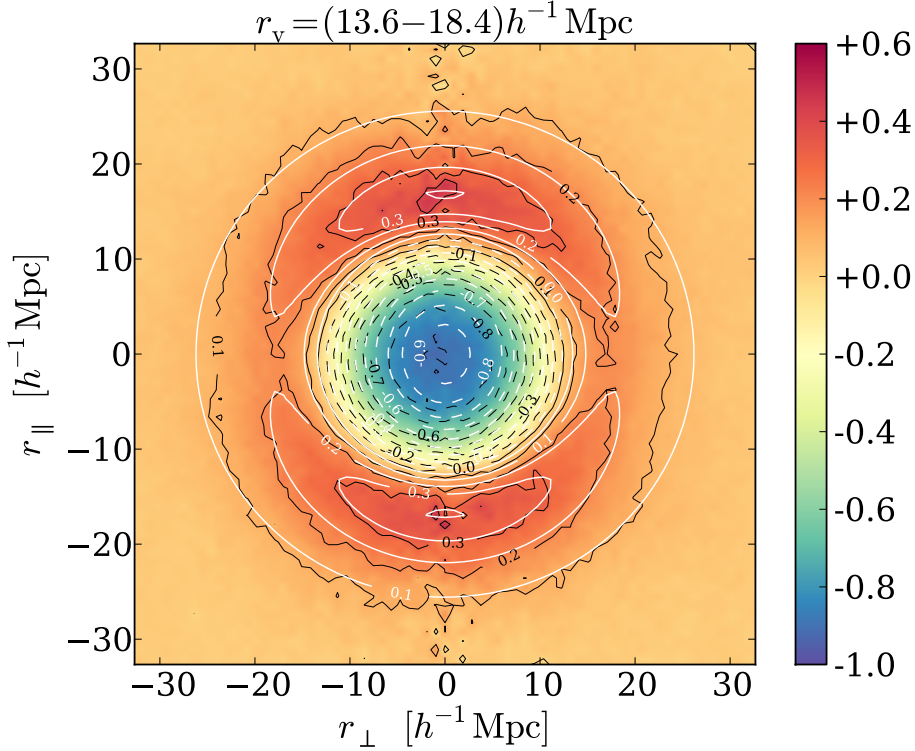


Figure 7: Void-galaxy cross-correlation function from a mock-galaxy catalog in redshift space. White contours show the best-fit Gaussian streaming model with use of equation (103). Adopted from Hamaus et al. (2015).

where the first equality describes the ensemble average over all individual void galaxy-density profiles and the second one represents a histogram of Dirac delta functions δ^D for the galaxy positions \mathbf{x}_j at separation \mathbf{r} from each void center \mathbf{X}_i . This expression can be written as a convolution of the number density of void centers n_v with the number density of galaxies n_g ,

$$\begin{aligned}
 V \sum_{i,j} \int \frac{1}{N_v} \delta^D(\mathbf{X}_i - \mathbf{x}) \frac{1}{N_g} \delta^D(\mathbf{x} - \mathbf{x}_j + \mathbf{r}) d^3x &= \\
 &= \frac{1}{V} \int \frac{n_v(\mathbf{x}) n_g(\mathbf{x} + \mathbf{r})}{\bar{n}_v \bar{n}_g} d^3x = 1 + \xi(r), \quad (123)
 \end{aligned}$$

where V is the total observed volume, $\bar{n}_v = N_v/V$, $\bar{n}_g = N_g/V$, and $\xi(r)$ denotes the void-galaxy cross-correlation function in real space.

Unfortunately, the average mass-density contrast $\Delta(r)$ around voids is not directly observable, but with the help of simulations it has been demonstrated that its relation to the corresponding average galaxy-density contrast $\bar{\xi}(r)$ is remarkably linear [Pollina et al. (2017)],

$$\bar{\xi}(r) = b\Delta(r) , \quad (124)$$

with a single galaxy-bias parameter b . Therefore, in exchanging $\Delta(r)$ with the observable $\bar{\xi}(r)$ in equation (119), we can absorb the bias parameter into the definition of the growth rate by defining the relative growth rate $\beta \equiv f/b$. Then, plugging this into equation (118), we have

$$\mathbf{s} = \mathbf{r} - \frac{\beta}{3} \hat{\mathbf{X}} \cdot \mathbf{r} \bar{\xi}(r) \hat{\mathbf{X}} . \quad (125)$$

The total number of galaxies cannot be altered by redshift-space distortions, therefore the void-galaxy cross-correlation functions in real and redshift space, ξ and ξ^s , must satisfy

$$\int [1 + \xi(r)] d^3r = \int [1 + \xi^s(\mathbf{s})] d^3s = \int [1 + \xi^s(\mathbf{r})] \det\left(\frac{\partial \mathbf{s}}{\partial \mathbf{r}}\right) d^3r . \quad (126)$$

In the last step we introduce the determinant of the Jacobian $\partial \mathbf{s} / \partial \mathbf{r}$ to perform a coordinate transformation between \mathbf{s} and \mathbf{r} . Using equation (125) the Jacobian equates to

$$\frac{\partial \mathbf{s}}{\partial \mathbf{r}} = \mathbb{1} - \frac{\beta}{3} \left[\bar{\xi}(r) \hat{\mathbf{X}} \hat{\mathbf{X}}^\top + \hat{\mathbf{X}} \cdot \mathbf{r} \frac{\partial \bar{\xi}(r)}{\partial \mathbf{r}} \hat{\mathbf{X}} \right] , \quad (127)$$

where $\mathbb{1}$ represents the unit matrix. Upon taking the determinant, we obtain

$$\det\left(\frac{\partial \mathbf{s}}{\partial \mathbf{r}}\right) = 1 - \frac{\beta}{3} \bar{\xi}(r) - \frac{\beta}{3} \hat{\mathbf{X}} \cdot \mathbf{r} \frac{\partial \bar{\xi}(r)}{\partial r} \frac{\mathbf{r}}{r} \cdot \hat{\mathbf{X}} , \quad (128)$$

where we made use of the identity $\partial r / \partial \mathbf{r} = \mathbf{r} / r$ and the determinant lemma

$$\det(\mathbf{A} + \mathbf{u}\mathbf{v}^\top) = \det \mathbf{A} (1 + \mathbf{v}^\top \mathbf{A}^{-1} \mathbf{u}) , \quad (129)$$

for any invertible square matrix \mathbf{A} and vectors \mathbf{u} , \mathbf{v} of the same dimension. The average galaxy-density contrast is an integral over the void-galaxy cross-correlation function,

$$\bar{\xi}(r) = \frac{3}{r^3} \int_0^r \xi(r') r'^2 dr' , \quad (130)$$

with $\partial\bar{\xi}(r)/\partial r = 3/r [\xi(r) - \bar{\xi}(r)]$. Defining the angle ϑ between the line-of-sight direction \mathbf{X} and the separation vector \mathbf{r} via

$$\cos \vartheta = \frac{\mathbf{X} \cdot \mathbf{r}}{|\mathbf{X}| |\mathbf{r}|} \equiv \mu , \quad (131)$$

the determinant of the Jacobian can be written as

$$\det \left(\frac{\partial \mathbf{s}}{\partial \mathbf{r}} \right) = 1 - \frac{\beta}{3} \bar{\xi}(r) - \beta \mu^2 [\xi(r) - \bar{\xi}(r)] . \quad (132)$$

Using this in equation (126) and solving for ξ^s to linear order in ξ and $\bar{\xi}$ finally yields a relation between the real-space and redshift-space void-galaxy cross-correlation functions,

$$\xi^s(r, \mu) = \xi(r) + \frac{\beta}{3} \bar{\xi}(r) + \beta \mu^2 [\xi(r) - \bar{\xi}(r)] . \quad (133)$$

As ξ^s is no longer isotropic, one can decompose the redshift-space correlation function into multipoles using the Legendre polynomials $P_\ell(\mu)$ via

$$\xi_\ell(r) = \int_0^1 \xi^s(r, \mu) (1 + 2\ell) P_\ell(\mu) d\mu . \quad (134)$$

The only non-vanishing multipoles of Eq. (133) are the monopole with $P_0 = 1$ and the quadrupole with $P_2 = (3\mu^2 - 1)/2$,

$$\xi_0(r) = \left(1 + \frac{\beta}{3} \right) \xi(r) , \quad (135)$$

$$\xi_2(r) = \frac{2\beta}{3} [\xi(r) - \bar{\xi}(r)] . \quad (136)$$

Hence, these two functions fully determine the void-galaxy cross-correlation

function in redshift space, which can then be expressed as

$$\xi^s(r, \mu) = \xi_0(r) + \frac{3\mu^2 - 1}{2} \xi_2(r). \quad (137)$$

The monopole and quadrupole are related via a simple linear equation,

$$\xi_0(r) - \bar{\xi}_0(r) = \xi_2(r) \frac{3 + \beta}{2\beta}, \quad (138)$$

which, given the multipole measurements, solely depends on the relative growth rate $\beta = f/b$. Figure 8 depicts measurements of these multipoles from galaxies and voids observed with the Sloan Digital Sky Survey (SDSS). The functional form of the quadrupole nicely agrees with the combination $\xi_0 - \bar{\xi}_0$, as predicted by equation (138). Figure 9 summarizes constraints on β from the LOWZ and CMASS samples of the SDSS, and compares them to the standard model expectations in cosmology.

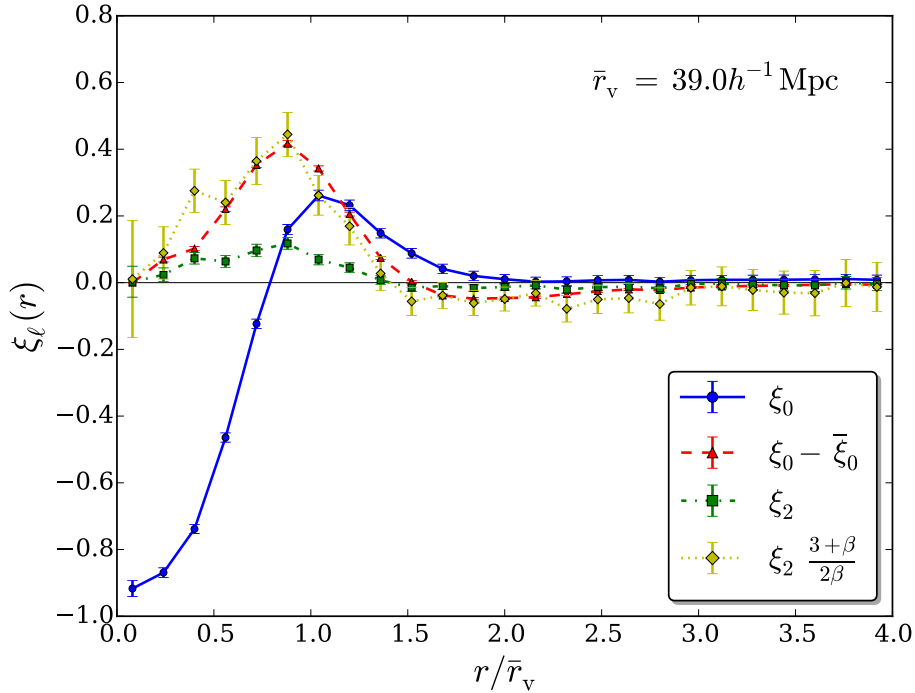


Figure 8: Multipoles of the void-galaxy cross-correlation function in the CMASS sample of the SDSS. Adopted from Hamaus et al. (2017).

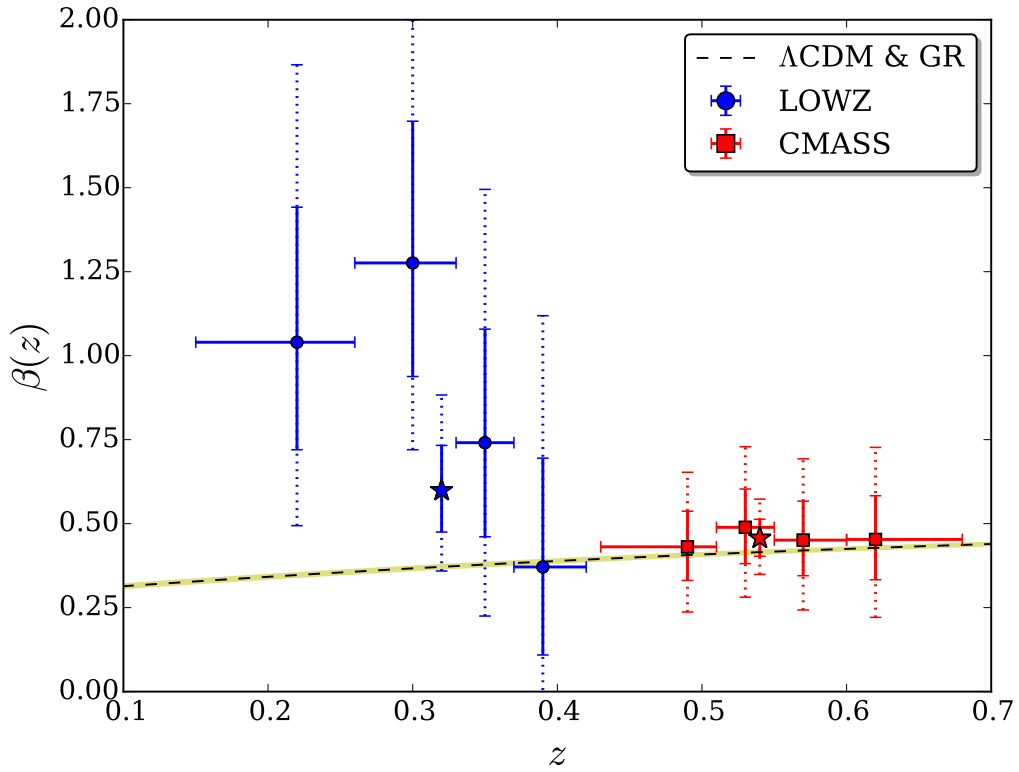


Figure 9: Growth rate constraints from LOWZ (blue circles) and CMASS (red squares). Stars represent the joint constraint from voids of all redshifts in each sample. Vertical solid lines indicate 1σ , dotted lines 2σ confidence intervals, and horizontal lines delineate redshift bins. The dashed line with yellow shading shows $\beta = \Omega_m^\gamma(z)/b$, with $\Omega_m(z=0) = 0.308 \pm 0.012$, $\gamma = 0.55$, and $b = 1.85$, assuming a flat Λ CDM cosmology and GR. Adopted from Hamaus et al. (2017).

4.2 Alcock-Paczyński test

4.3 Weak lensing

4.4 Integrated Sachs-Wolfe effect

References

- Bardeen, J. M., Bond, J. R., Kaiser, N., and Szalay, A. S. (1986). The statistics of peaks of Gaussian random fields. *Astrophys. J.*, 304:15–61.
- Bernardeau, F. (1994). The nonlinear evolution of rare events. *Astrophys. J.*, 427:51–71.
- Bertschinger, E. (1985). The self-similar evolution of holes in an Einstein-de Sitter universe. *ApJS*, 58:1–37.
- Blumenthal, G. R., da Costa, L. N., Goldwirth, D. S., Lecar, M., and Piran, T. (1992). The largest possible voids. *Astrophys. J.*, 388:234–241.
- Bond, J. R., Cole, S., Efstathiou, G., and Kaiser, N. (1991). Excursion set mass functions for hierarchical Gaussian fluctuations. *Astrophys. J.*, 379:440–460.
- Cooray, A. and Sheth, R. (2002). Halo models of large scale structure. *Phys. Rep.*, 372:1–129.
- Eke, V. R., Cole, S., and Frenk, C. S. (1996). Cluster evolution as a diagnostic for Omega. *Mon. Not. Roy. Astron. Soc.*, 282.
- Fisher, K. B. (1995). On the Validity of the Streaming Model for the Redshift-Space Correlation Function in the Linear Regime. *Astrophys. J.*, 448:494.
- Gunn, J. E. and Gott, III, J. R. (1972). On the Infall of Matter Into Clusters of Galaxies and Some Effects on Their Evolution. *Astrophys. J.*, 176:1.
- Hamaus, N., Cousinou, M.-C., Pisani, A., Aubert, M., Escoffier, S., and Weller, J. (2017). Multipole analysis of redshift-space distortions around cosmic voids. *ArXiv e-prints*.
- Hamaus, N., Pisani, A., Sutter, P. M., Lavaux, G., Escoffier, S., Wandelt, B. D., and Weller, J. (2016). Constraints on Cosmology and Gravity from the Dynamics of Voids. *Physical Review Letters*, 117(9):091302.

- Hamaus, N., Sutter, P. M., Lavaux, G., and Wandelt, B. D. (2015). Probing cosmology and gravity with redshift-space distortions around voids. *JCAP*, 11:036.
- Hamaus, N., Sutter, P. M., and Wandelt, B. D. (2014a). Universal Density Profile for Cosmic Voids. *Physical Review Letters*, 112(25):251302.
- Hamaus, N., Wandelt, B. D., Sutter, P. M., Lavaux, G., and Warren, M. S. (2014b). Cosmology with Void-Galaxy Correlations. *Physical Review Letters*, 112(4):041304.
- Jennings, E., Li, Y., and Hu, W. (2013). The abundance of voids and the excursion set formalism. *Mon. Not. Roy. Astron. Soc.*, 434:2167–2181.
- Kaiser, N. (1987). Clustering in real space and in redshift space. *Mon. Not. Roy. Astron. Soc.*, 227:1–21.
- Lacey, C. and Cole, S. (1993). Merger rates in hierarchical models of galaxy formation. *Mon. Not. Roy. Astron. Soc.*, 262:627–649.
- Lahav, O., Lilje, P. B., Primack, J. R., and Rees, M. J. (1991). Dynamical effects of the cosmological constant. *Mon. Not. Roy. Astron. Soc.*, 251:128–136.
- Peebles, P. J. E. (1980). *The large-scale structure of the universe*.
- Pollina, G., Hamaus, N., Dolag, K., Weller, J., Baldi, M., and Moscardini, L. (2017). On the linearity of tracer bias around voids. *Mon. Not. Roy. Astron. Soc.*, 469:787–799.
- Press, W. H. and Schechter, P. (1974). Formation of Galaxies and Clusters of Galaxies by Self-Similar Gravitational Condensation. *Astrophys. J.*, 187:425–438.
- Ronconi, T. and Marulli, F. (2017). Towards a cosmological exploitation of cosmic void statistics - New numerical tools in the CosmoBolognaLib to extract cosmological constraints from the void size function. *ArXiv e-prints*.

Sheth, R. K. (1998). The generalized Poisson distribution and a model of clustering from Poisson initial conditions. *Mon. Not. Roy. Astron. Soc.*, 299:207–217.

Sheth, R. K. and van de Weygaert, R. (2004). A hierarchy of voids: much ado about nothing. *Mon. Not. Roy. Astron. Soc.*, 350:517–538.

Zentner, A. R. (2007). The Excursion Set Theory of Halo Mass Functions, Halo Clustering, and Halo Growth. *International Journal of Modern Physics D*, 16:763–815.